Energy- and Momentum-Resolved Photoelectron Spin Polarization in Multiphoton Ionization of Xe by Circularly Polarized Fields

Ming-Ming Liu,[1] Yun Shao,[1] Meng Han,[1] Peipei Ge,[1] Yongkai Deng,[1] Chengyin Wu,[1,3,4] Qihuang Gong,[1,3,4] and Yunquan Liu[1,2,3,4,*]

[1]*School of Physics and State Key Laboratory for Mesoscopic Physics, Peking University, Beijing 100871, China*
[2]*HEDPS, Center for Applied Physics and Technology, Peking University, Beijing 100084, China*
[3]*Collaborative Innovation Center of Quantum Matter, Beijing 100871, China*
[4]*Collaborative Innovation Center of Extreme Optics, Shanxi University, Taiyuan, Shanxi 030006, China*

(Received 29 August 2017; published 24 January 2018)

We perform a joint experimental and theoretical study on momentum- and energy-resolved photoelectron spin polarization in multiphoton ionization of Xe atoms by circularly polarized fields. We experimentally measure the photoelectron momentum distributions of Xe atoms in circularly polarized near-infrared (800 nm) and ultraviolet (400 nm) light, respectively. We analyze the momentum- and energy-resolved photoelectron spin polarization by comparing the experimental photoelectron momentum distributions with the simulations, although we cannot derive the spin polarization solely from the experiment. We show that the use of circularly polarized ultraviolet light at 400 nm can create better than 90% spin polarization with focal volume effect considered, which enables the separation of the spin states by momentum gating. This paves the way to produce high-degree spin-polarized electron sources from strong-field multiphoton ionization.

DOI: 10.1103/PhysRevLett.120.043201

Spin is one of the intrinsic properties of electrons [1]. Ever since its discovery, considerable effort has been devoted to the study of producing spin-polarized electrons because of its wide applications [2]. For example, few-photon photoionization by circularly polarized pulses is one of the approaches to produce spin-polarized electrons. Fano first theoretically demonstrated that single-photon ionization of atoms in circularly polarized light could lead to the generation of electrons with a high degree of spin polarization [3]. Subsequently, Lambropoulos theoretically studied that spin-polarized currents were possible to be produced via two- or three-photon ionization of alkali atoms [4,5], or by selective laser-induced interference [6] (for a review see, e.g., Ref. [7]).

Strong-field tunneling ionization is a particularly important phenomenon in ultrafast laser physics [8]. Recently, the role of electron's spin in strong-field ionization has attracted much attention. In 2013, Barth and Smirnova theoretically predicted that spin-polarized photoelectrons could be produced through tunneling ionization of the valent p shell of rare gas atoms in strong circularly polarized laser fields [9]. In the strong-field regime, spin polarization of photoelectrons is a consequence of spin-orbit coupling and the selective ionization of p states with different magnetic quantum numbers of rare gases [10–13] and molecules [14,15] in circularly polarized light. Besides direct ionization electrons, spin-polarized electrons were also expected to be produced in electron-ion recollision driven by intense tailored fields [16,17].

Most of the previous works focused on theoretical study to produce spin-polarized electrons. Very recently, Hartung *et al.* [18] performed a benchmark experiment in which they measured the energy-resolved spin polarization of photoelectrons of Xe atoms in circularly polarized light in an over-the-barrier regime at the wavelength of 800 nm. In this experiment, up to 30% of spin polarization depending on the photoelectron kinetic energy was observed. A higher degree of spin polarization is demanded for practical application and it would be very necessary to resolve the differential momentum distributions of spin-polarized photoelectrons.

In this Letter, we perform a combined experimental and theoretical study on the momentum- and energy-resolved spin polarization of photoelectrons in strong-field ionization of Xe atoms in circularly polarized near-infrared (800 nm) and ultraviolet (400 nm) light. In near-infrared light (800 nm), we do not observe well separated above threshold ionization (ATI) [19] peaks of photoelectrons. Instead, there are two sets of separated ATI peaks originating from the spin-orbit coupling effect in circularly polarized ultraviolet light (400 nm). We analyze the momentum-resolved photoelectron spin polarization by the simulation, although we cannot obtain the information of spin polarization solely from the experiment. In near-infrared light, we show that the degree of spin polarization is less than 40%, and the spin-up and spin-down electrons cannot be separated. While in ultraviolet light, the degree of photoelectron spin polarization can be extremely high (~90% with focal volume effect considered).

Experimentally, we use cold-target recoil ion momentum spectroscopy to measure the three-dimensional momentum of photoelectrons [20]. The frequency of the near-infrared laser pulse (25 fs, 800 nm) is doubled with a 250-μm-thick β-barium-borate crystal to produce the 400 nm ultraviolet laser pulse. The pulse duration at 400 nm is ~50 fs. Then we use a pair of half and quarter wave plates to produce circularly polarized light. The rotation of the wave plates is precisely controlled with a motorized rotator to guarantee a perfect circular polarization at both wavelengths. The laser pulse is focused onto the supersonic gas beam by a silver concave mirror ($f = 75$ mm). The electrons and ions are detected with two separate time- and position-sensitive microchannel plate detectors in a time-of-flight spectrometer. We analyze the photoelectrons coincident with singly charged ions to avoid false signals.

In Fig. 1, we show the measured (blue solid line) and simulated (black solid line) energy spectra of photoelectrons in circularly polarized near-infrared light at 800 nm. The effective laser intensity in the experiment is $\sim 0.75 \times 10^{14}$ W/cm^2, which is calibrated by comparing the measured energy spectrum with the simulated results at a series of laser intensities. The Keldysh parameter $\gamma = (\sqrt{2I_p})\omega/E_0$ (I_p is the ionization potential, ω is field frequency, E_0 is field amplitude, atomic units are used throughout unless otherwise specified) is ~1.65. The calculated energy spectra of spin-up (green dashed line) and spin-down (red dash-dotted line) photoelectrons are also shown in Fig. 1.

When rare gas atoms are exposed to strong laser field, the measured energy spectra are expected to exhibit discrete ATI peaks [19]. However, in the measured energy spectrum at 800 nm, we do not see evident ATI peaks. On the other hand, due to spin-orbit coupling, when rare gas atoms are ionized at the multiphoton ionization regime, the produced photoelectron spectra are expected to show two sets of ATI peaks corresponding to different ionic states ($^2P_{3/2}$, $^2P_{1/2}$). For Xe atoms, the separation is 1.31 eV. In circularly polarized light at 800 nm, we do not observe this energy separation either.

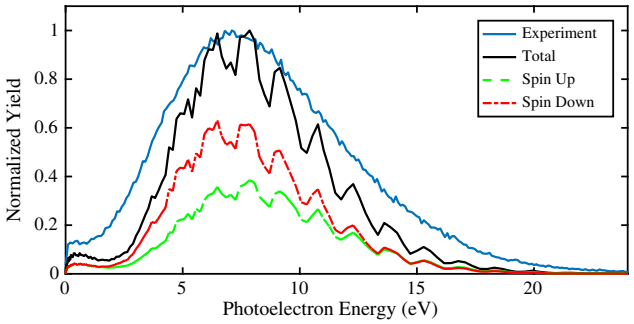

FIG. 1. The measured (blue solid line) and simulated (black solid line) photoelectron energy spectra in near-infrared circularly polarized light at 800 nm. The maximum data have been normalized to unity. The green dashed line and red dash-dotted line represent the simulated energy distributions of spin-up and spin-down electrons, respectively. Focal volume effect has been taken into account.

In order to analyze the property of electron spin polarization, we have extended the strong-field approximation [21–25] to simulate the ionization of Xe atoms from different atomic orbitals. Within the strong-field approximation, the direct transition amplitude from field-free bound state to Volkov state is $M(\mathbf{p}) = -i\int_{t_i}^{t_f} dt\langle \mathbf{p}+\mathbf{A}(t)|\mathbf{r}\cdot\mathbf{E}(t)|\varphi_{nlm_l}\rangle e^{iS(t)}$. Here, t_i and t_f are the arriving and departing time of the laser pulse, respectively. $\mathbf{E}(t)$ is the instantaneous laser electric field and $\mathbf{A}(t)$ is the corresponding vector potential. $\mathbf{p}$ is the canonical momentum, φ_{nlm_l} is the hydrogenlike atomic wave function in coordinate representation, and n, l, m_l are the principal, orbital, and magnetic quantum numbers, respectively. $S(t) = \int_0^t d\tau[\frac{1}{2}[\mathbf{p}+\mathbf{A}(\tau)]^2 + I_p]$ is the classical action. Using Fourier transform, one can rewrite the transition amplitude as

$$\begin{aligned} M(\mathbf{p}) &= -i\int_{t_i}^{t_f} dt\langle \mathbf{p}+\mathbf{A}(t)|\mathbf{r}\cdot\mathbf{E}(t)|\varphi_{nlm_l}\rangle e^{iS(t)} \\ &= -i\int_{t_i}^{t_f} dt\left(\int d\mathbf{r}e^{-i\mathbf{q}\cdot\mathbf{r}}\mathbf{r}\varphi_{nlm_l}(\mathbf{r})\right)\cdot\mathbf{E}(t)e^{iS(t)} \\ &= -i\int_{t_i}^{t_f} dt\left(\int id\mathbf{r}\frac{\partial}{\partial\mathbf{q}}(e^{-i\mathbf{q}\cdot\mathbf{r}})\varphi_{nlm_l}(\mathbf{r})\right)\cdot\mathbf{E}(t)e^{iS(t)} \\ &= \int_{t_i}^{t_f} dt\frac{\partial}{\partial\mathbf{q}}\left(\int d\mathbf{r}e^{-i\mathbf{q}\cdot\mathbf{r}}\varphi_{nlm_l}(\mathbf{r})\right)\cdot\mathbf{E}(t)e^{iS(t)} \\ &= \int_{t_i}^{t_f} dt\frac{\partial}{\partial\mathbf{q}}[\phi_{nlm_l}(\mathbf{q})]\cdot\mathbf{E}(t)e^{iS(t)}. \end{aligned} \tag{1}$$

Here, $\mathbf{q} = \mathbf{p} + \mathbf{A}(t)$, and ϕ_{nlm_l} is the hydrogenlike atomic wave function in momentum representation [26,27]. We do the time integration in Eq. (1) numerically to obtain the transition amplitude from valence $5p$ orbitals of Xe with specific magnetic quantum numbers. The squared modulus of the transition amplitude represents the yield of photoelectrons with a certain canonical momentum, $w(\mathbf{p}) = |M(\mathbf{p})|^2 d\mathbf{p}$.

The atomic orbitals used in Eq. (1) are the simultaneous eigenstates of the square of orbital angular momentum $\boldsymbol{l}^2$, and its component l_z, which have a specific magnetic quantum number. Because of spin-orbit coupling, the valence $5p$ orbitals of Xe atoms are no longer degenerate, and the magnetic quantum number is no longer a conservative variable. When removing the valence electron, the ion could be populated at the state of $^2P_{3/2}$ or $^2P_{1/2}$, and the corresponding ionization potentials are $I_p^{^2P_{3/2}} = 12.13$ eV and $I_p^{^2P_{1/2}} = 13.44$ eV, respectively. To include the spin-orbit coupling, we superpose the ionization contribution from atomic orbitals with different magnetic

quantum numbers. The relative weight is determined by the Clebsch-Gordan coefficients. According to the relation between the spin and orbital angular momenta, one can further infer the spin of photoelectrons. The rates of spin-up and spin-down photoelectrons are given by [9,16]

$$w_\uparrow(\mathbf{p}) = \frac{2}{3}w(\mathbf{p}; I_p^{^2P_{1/2}}, m_l = -1) + \frac{1}{3}w(\mathbf{p}; I_p^{^2P_{3/2}}, m_l = -1) + w(\mathbf{p}; I_p^{^2P_{3/2}}, m_l = 1),$$
$$w_\downarrow(\mathbf{p}) = \frac{2}{3}w(\mathbf{p}; I_p^{^2P_{1/2}}, m_l = 1) + \frac{1}{3}w(\mathbf{p}; I_p^{^2P_{3/2}}, m_l = 1) + w(\mathbf{p}; I_p^{^2P_{3/2}}, m_l = -1). \quad (2)$$

In the simulation, we use a right circularly polarized laser light and the vector potential is given by $\mathbf{A}(t) = (E_0/\omega)\exp[-4\ln 2t^2/(\tau_{\mathrm{FWHM}}^2)][\sin(\omega t)\mathbf{e}_x - \cos(\omega t)\mathbf{e}_y]$. Here, E_0 is the laser electric field amplitude, ω is the laser frequency, and τ_{FWHM} is the full width at half maximum of the pulse envelope (in the simulation,τ_{FWHM} is 26.7 fs). In the simulation, we neglect the contribution of atomic orbitals with magnetic quantum number $m_l = 0$, because it is strongly suppressed in polarization plane.

The agreement of the envelope of energy spectrum between the measurement and simulation is good, except that the sharp ATI peaks appear in the simulated spectrum. This is mostly because in circularly polarized light at 800 nm more than eight photons are necessary be absorbed to free the valence electron. Many excited states contribute to the ionization and this will wash out the ATI peaks. This interpretation is further supported by the measured and calculated electron momentum distributions in the laser polarization plane, as shown in Figs. 2(a) and 2(b). The measured momentum distribution does not have any interference structures, but the calculated spectrum has clear ATI structure. In Fig. 2(b), we sum up the contribution from both spin-up and spin-down electrons. One might expect that the focal averaging effect might wash out the ATI peaks. However, we have included the focal averaging effect in the simulation. The relative weight of each intensity is given by $dV/dI \propto (I_0 + 2I)\sqrt{I_0 - I}/I^{5/2}$ (I_0 is the peak intensity). The ATI peaks still survive in the calculated momentum distribution. On the other hand, in the simulation, there are no excited states included.

In Figs. 2(c) and 2(d), we show the simulated momentum distributions of the spin-up and spin-down photoelectrons at 800 nm, respectively. The yields of spin-down electrons are much more than those of spin-up electrons. The relative contributions of photoelectrons with different spin will reverse if one uses a left circularly polarized light. Comparing Figs. 2(c) with 2(d), one can see that the radius of the doughnutlike momentum distribution for spin-up electrons is slightly larger than that of spin-down electrons. The difference in yields and momentum distributions for photoelectrons with different spin originates from two reasons. One is that, in right circularly polarized light, the atomic p orbital with magnetic quantum number $m_l = -1$ counterrotates with the circularly polarized light and is much easier to be removed. The other is that, due to spin-orbit coupling, spin and orbital angular momenta are related with each other according to the conservation of total angular momentum, and thus the selective ionization of orbitals with different magnetic quantum numbers leads to spin polarization of photoelectrons.

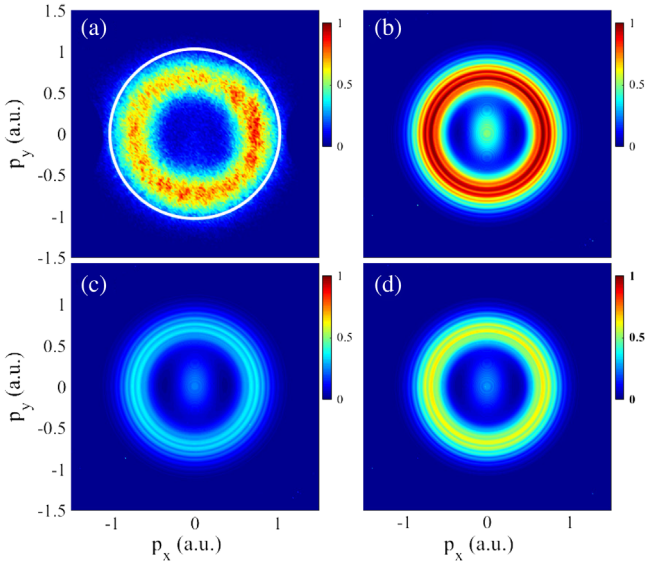

FIG. 2. Measured (a) and simulated (b) two-dimensional photoelectron momentum distributions in laser polarization plane corresponding to the energy spectra in Fig. 1. The maximum data have been normalized to be unity. For the measured distribution we restrict the momentum along the laser propagation direction so that $|p_z| < 0.1$ (a.u.). The white circle in (a) indicates the position of the transition point of spin polarization. (c),(d) Simulated momentum distributions of spin-up and spin-down electrons, respectively.

Photoelectron spin polarization with respect to energy was measured for Xe atoms in circularly polarized light at 800 nm in the benchmark experiment [18]. However, one cannot separate the spin-up and spin-down electrons at 800 nm. In order to proceed to practical application, it would be necessary to resolve the momentum distribution of spin-polarized photoelectrons. In Figs. 3(a) and 3(b), we show the simulated momentum- and energy-resolved spin polarization of photoelectrons. The momentum-resolved spin polarization is defined as

$$\mathrm{SP}(\mathbf{p}) = \frac{w_\uparrow(\mathbf{p}) - w_\downarrow(\mathbf{p})}{w_\uparrow(\mathbf{p}) + w_\downarrow(\mathbf{p})}. \quad (3)$$

The energy-resolved spin polarization has a similar definition as in Ref. [18]. One can see that the spin polarization changes from negative to positive as the energy (or momentum) of photoelectrons increases. For photoelectrons with low or high momentum, the degree of spin polarization is relatively high (up to 40%), while for

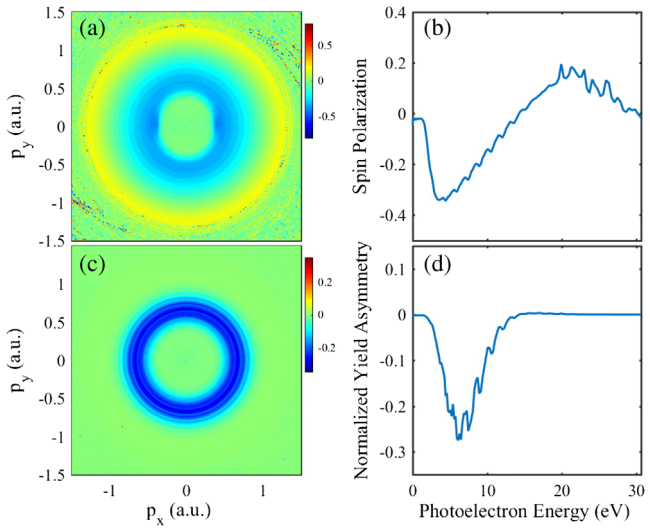

FIG. 3. (a),(b) Calculated 2D momentum- and energy- resolved spin polarization. (c),(d) The corresponding momentum- and energy-resolved normalized yield asymmetry, respectively. Both the spin polarization and the normalized yield asymmetry are obtained from the simulation.

photoelectrons with moderate momentum, the degree of spin polarization is low. There is a transition point of the sign of spin polarization, which is about 14.5 eV in energy (or 1.03 a.u. in momentum). In Fig. 2(a), the white circle indicates the transition in the measured momentum distribution, which is slightly larger than the most probable momentum.

When the momentum is large or small, although the photoelectrons have a high degree of spin polarization, the photoelectron yields can be quite small. To take account of the yields, we have further calculated the momentum- and energy-resolved normalized yield asymmetry between photoelectrons with different spin. The momentum-resolved normalized yield asymmetry is defined as [15]

$$\mathrm{NYA}(\mathbf{p}) = \frac{w_\uparrow(\mathbf{p}) - w_\downarrow(\mathbf{p})}{\mathrm{MAX}[w_\uparrow(\mathbf{p}) + w_\downarrow(\mathbf{p})]}. \tag{4}$$

The normalized yield asymmetry in Eq. (4) reflects the relative abundance of electrons with different spin polarization at a specific momentum. As shown in Figs. 3(c) and 3(d), one can see that at the most probable momentum photoelectrons possess a negative spin polarization. Because of lower ionization potential, most of the electrons are from the ionic state of $^2P_{3/2}$. And because of the fourfold degeneracy of $^2P_{3/2}$, the degree of spin polarization from this ionization channel cannot exceed 50% [9]. Summing up the contributions of $^2P_{3/2}$ and $^2P_{1/2}$ channels, the spin polarization decreases even further. The overall spin-polarization degree is less than 40% at 800 nm. More crucially, one cannot separate the spin-up and spin-down electrons well.

The ability to separate photoelectron spectra corresponding to $^2P_{3/2}$ and $^2P_{1/2}$ ionization channels experimentally will offer the opportunity to achieve a high degree of spin polarization of the coherent electron source. The energy separation has been observed in multiphoton ionization by linearly polarized fields [28,29]; however, there is no spin polarization effect using linearly polarized fields. Thus, we turn to study the spin polarization of photoelectrons in circularly polarized ultraviolet light at 400 nm.

In Figs. 4(a) and 4(b), we show the measured and simulated momentum distributions in circularly polarized ultraviolet laser light, respectively. The effective laser intensity in the experiment is $\sim 0.75 \times 10^{14}$ W/cm^2, and the Keldysh parameter γ is ~ 3.29. At 400 nm, the experiment and simulation have an excellent agreement. One can see that there are two sets of concentric ATI peaks with an energy interval of 1.31 eV, which originate from $^2P_{3/2}$ or $^2P_{1/2}$ channels, respectively. Both sets of ATI peaks can be seen clearly. Because of the higher ionization potential of the $^2P_{1/2}$ channel, the momentum or energy corresponding to the first-order ATI is smaller than that of the $^2P_{3/2}$ channel. In Figs. 4(c) and 4(d), we illustrate the calculated momentum distributions of spin-up and spin-down photoelectrons, respectively. For spin-up photoelectrons, the contributions from $^2P_{3/2}$ and $^2P_{1/2}$ channels are comparable. However, for spin-down photoelectrons, the contribution of the $^2P_{3/2}$ channel dominates, and the yields

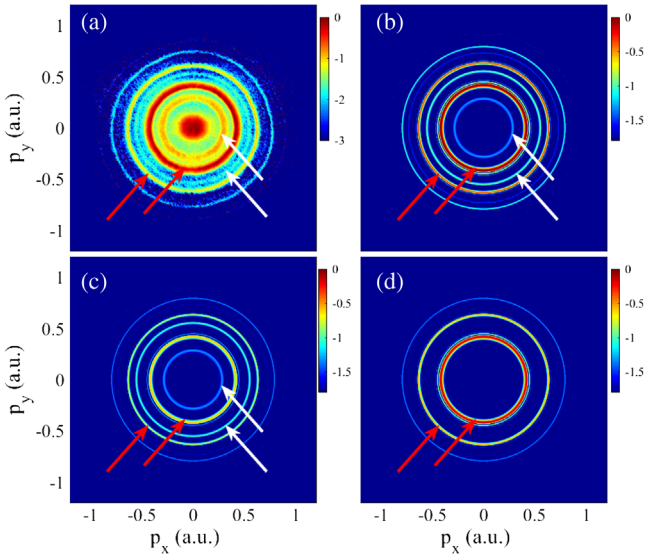

FIG. 4. The measured (a) and simulated (b) 2D photoelectron momentum distributions in laser polarization plane in ultraviolet circularly polarized light at 400 nm. For the measured distribution we restrict the momentum along the laser propagation direction so that $|p_z| < 0.1$ (a.u.). (c),(d) Simulated momentum distribution of spin-up and spin-down electrons, respectively. Red arrows indicate the ATI peaks corresponding to the $^2P_{3/2}$ channel, and white arrows indicate those corresponding to the $^2P_{1/2}$ channel. Both the measured and simulated spectra are in logarithmic scale.

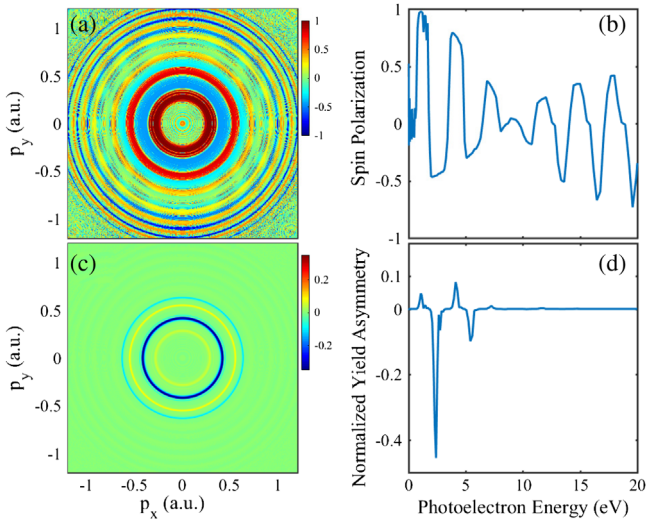

FIG. 5. (a),(b) 2D momentum- and energy-resolved spin polarization in ultraviolet circularly polarized light at 400 nm, respectively. (c),(d) The corresponding momentum- and energy-resolved normalized yield asymmetry. Both the spin polarization and the normalized yield asymmetry are obtained from the simulation.

from the $^2P_{1/2}$ channel are quite weak. That is because, in right circularly polarized light, the counterrotating electronic orbital ($m = -1$) is much easier to be ionized. According to Eq. (2), one can see that for spin-up photoelectrons, both $^2P_{3/2}$ and $^2P_{1/2}$ channels will contribute, while for spin-down photoelectrons, only the $^2P_{3/2}$ channel has a counterrotating component and thus will dominate.

In Figs. 5(a) and 5(b), we show the momentum- and energy-resolved spin polarization of photoelectrons at 400 nm. One can see that the spin polarization oscillates as the energy (or momentum) increases. This oscillation originates from the separation of photoelectrons from different ionization channels. In right circularly polarized light, the first-order ATI photoelectrons from the $^2P_{1/2}$ channel have positive spin polarization, while the first-order ATI photoelectrons from the $^2P_{3/2}$ channel have negative spin polarization. There is a transition point of energy-resolved spin polarization at about 8.6 eV, where the amplitude of the oscillation reaches the minimum. Beyond this transition point, the spin polarization for each channel changes its sign, and the yield of photoelectrons also decreases rapidly. The spin polarization for the first ATI photoelectron from the $^2P_{1/2}$ channel can reach 97% at the energy of 1.1 eV. Even if we include the focal volume effect, the spin polarization is still higher than 90%. In Figs. 5(c) and 5(d), we show the corresponding normalized yield asymmetry. One can see that the yields of spin-down electrons dominate the distribution, which is similar to the result at 800 nm. At the energy of 2.4 eV (the first-order ATI energy peak from the $^2P_{3/2}$ channel), the spin polarization decreases to ~45% where the photoelectron yield reaches the maximum.

The second ATI related with the $^2P_{1/2}$ ionic state has an energy of ~4.2 eV. The spin polarization has decreased to 75%. However, for the second ATI related with $^2P_{3/2}$, spin polarization decreases further to ~30%. We note that at 400 nm, many near-zero-momentum populations appear in the momentum distribution, but it is not captured by the simulation. Those electrons are mostly from four photon ionization channels, which are related to the $^2P_{3/2}$ ionic states. The spin polarization would be around ~50%.

In conclusion, we present the first experiment to study the momentum distributions of photoelectrons by multiphoton ionization of Xe atoms in circularly polarized near-infrared and ultraviolet light. In the near-infrared field, we can observe neither the ATI peaks nor the separation of $^2P_{3/2}$ and $^2P_{1/2}$ ionization channels. The overall spin polarization of photoelectrons is less than 40%. Using the ultraviolet circularly polarized light, we show that the momentum-resolved spin polarization can reach as high as ~90% if considering focal volume effect. The results indicate that spin-polarized photoelectrons can be obtained by momentum gating in multiphoton ionization processes using circularly polarized ultraviolet light. Photoelectron spin polarization is essentially dependent on the wavelength of the driving laser. Producing photoelectrons with a high degree of spin polarization can open a new direction of introducing polarized low-energy electron diffraction [30], to probing the magnetic properties of condensed matters [31], and to be a source of polarized electron accelerators.

This work is supported by the National Science Foundation of China (Grants No. 11434002, No. 11774013, and No. 11527901).

Note added in proof.—Recently, the spin polarization of multiphoton ionization Xe atoms at 395 nm was measured via time-of-flight (TOF)-Mott polarimeter [32]. It was also found that the spin polarization from $J = 1/2$ channel is opposite and is higher than that from $J = 3/2$ channel, and it was shown that the ionization probability is strongly dependent on the sign of the magnetic quantum number. Generally, the conclusion agrees with this work if considering the resolution and the acceptance angle of TOF-Mott polarimeter.

*Yunquan.liu@pku.edu.cn

[1] G. E. Uhlenbeck and S. Goudsmit, Nature (London) **117**, 264 (1926).
[2] R. Wiesendanger, Rev. Mod. Phys. **81**, 1495 (2009).
[3] U. Fano, Phys. Rev. **178**, 131 (1969).
[4] P. Lambropoulos, Phys. Rev. Lett. **30**, 413 (1973).
[5] P. Lambropoulos, J. Phys. B **7**, L33 (1974); T. Nakajima and P. Lambropoulos, Europhys. Lett. **57**, 25 (2002).
[6] S. N. Dixit, P. Lambropoulos, and P. Zoller, Phys. Rev. A **24**, 318 (1981).

[7] U. Heinzmann and J. H. Dil, J. Phys. Condens. Matter **24**, 173001 (2012).
[8] L. V. Keldysh, Zh. Eksp. Teor. Fiz. **47**, 1945 (1964) [Sov. Phys. JETP **20**, 1307 (1965)].
[9] I. Barth and O. Smirnova, Phys. Rev. A **88**, 013401 (2013).
[10] I. Barth and O. Smirnova, Phys. Rev. A **84**, 063415 (2011).
[11] I. Barth and O. Smirnova, Phys. Rev. A **87**, 013433 (2013).
[12] I. Barth and M. Lein, J. Phys. B **47**, 204016 (2014).
[13] T. Herath, L. Yan, S. K. Lee, and W. Li, Phys. Rev. Lett. **109**, 043004 (2012).
[14] K. Liu and I. Barth, Phys. Rev. A **94**, 043402 (2016).
[15] K. Liu, K. Renziehausen, and I. Barth, Phys. Rev. A **95**, 063410 (2017).
[16] D. B. Milošević, Phys. Rev. A **93**, 051402(R) (2016); J. Phys. B **50**, 164003 (2017).
[17] D. Ayuso, A. Jiménez-Galán, F. Morales, M. Ivanov, and O. Smirnova, New J. Phys. **19**, 073007 (2017).
[18] A. Hartung, F. Morales, M. Kunitski, K. Henrichs, A. Laucke, M. Richter, T. Jahnke, A. Kalinin, M. Schöffler, L. Ph. H. Schmidt, M. Ivanov, O. Smirnova, and R. Dörner, Nat. Photonics **10**, 526 (2016).
[19] P. Agostini, F. Fabre, G. Mainfray, G. Petite, and N. K. Rahman, Phys. Rev. Lett. **42**, 1127 (1979).
[20] J. Ullrich, R. Moshammer, A. Dorn, R. Dorner, L. Ph. H. Schmidt, and H. Schmidt-Bocking, Rep. Prog. Phys. **66**, 1463 (2003).
[21] A. M. Perelomov, V. S. Popov, and M. V. Terent'ev, Zh. Eksp. Teor. Fiz. **50**, 1393 (1966) [Sov. Phys. JETP **23**, 924 (1966)].
[22] F. H. M. Faisal, J. Phys. B **6**, L89 (1973).
[23] H. Reiss, Phys. Rev. A **22**, 1786 (1980).
[24] D. B. Milošević, G. G. Paulus, D. Bauer, and W. Becker, J. Phys. B **39**, R203 (2006).
[25] M. M. Liu, M. Li, Y. Shao, M. Han, Q. Gong, and Y. Liu, Phys. Rev. A **96**, 043410 (2017).
[26] B. Podolsky and L. Pauling, Phys. Rev. **34**, 109 (1929).
[27] J. C. Slater, Phys. Rev. **36**, 57 (1930).
[28] H. Rottke, J. Ludwig, and W. Sandner, J. Phys. B **29**, 1479 (1996).
[29] P. Kaminski, R. Wiehle, V. Renard, A. Kazmierczak, B. Lavorel, O. Faucher, and B. Witzel, Phys. Rev. A **70**, 053413 (2004).
[30] D. T. Pierece, R. J. Celotta, G.-C Wang, W. N. Unertl, A. Galejs, C. E. Kuyatt, and S. R. Mielczarek, Rev. Sci. Instrum. **51**, 478 (1980).
[31] S. A. Wolf, D. D. Awschalom, R. A. Buhrman, J. M. Daughton, S. von Molnár, M. L. Roukes, A. Y. Chtchelkanova, and D. M. Treger, Science **294**, 1488 (2001).
[32] D. Trabert, A. Hartung, S. Eckart, F. Trinter, A. Kalinin, M. Schöffler, L. Ph. H. Schmidt, T. Jahnke, M. Kunitski, and R. Dörner, following Letter, Phys. Rev. Lett. **120**, 043202 (2018).